M. Sánchez-Sanz · A.L. Sánchez · A. Liñán

Variable-density jet flows induced by concentrated sources of momentum and energy

Abstract The planar and axisymmetric variable-density flows induced in a quiescent gas by a concentrated source of momentum that is simultaneously either a source or a sink of energy are investigated for application to the description of the velocity and temperature far fields in laminar gaseous jets with either large or small values of the initial jet-to-ambient temperature ratio. The source fluxes of momentum and heat are used to construct the characteristic scales of velocity and length in the region where the density differences are of the order of the ambient density, which is slender for the large values of the Reynolds number considered herein. The problem reduces to the integration of the dimensionless boundary-layer conservation equations, giving a solution that depends on the gas transport properties but is otherwise free of parameters. The boundary conditions at the jet exit for integration are obtained by analysing the self-similar flow that appears near the heat source in planar and axisymmetric configurations and also near the heat sink in the planar case. Numerical integrations of the boundary-layer equations with these conditions give solutions that describe accurately the velocity and temperature fields of very hot planar and round jets and also of very cold plane jets in the far field region where the density and temperature differences are comparable to the ambient values. Simple scaling arguments indicate that the point source description does not apply, however, to cold round jets, whose far field region is not large compared with the jet development region, as verified by numerical integrations.

Keywords Point source · Laminar jet · Boundary-layer approximation · Gaseous flow

1 Introduction

The structure of the flow field resulting from the discharge of a gas stream of radius a into an atmosphere of the same gas is known to depend on the value of the jet Reynolds number $Re_j = \rho'_j u'_j a / \mu'_j$, where ρ'_j and μ'_j are the density and viscosity of the discharging gas and u'_j is the characteristic value of the velocity at the exit. For values of Re_j sufficiently larger than unity, the resulting flow is slender and can be correspondingly

M. Sánchez-Sanz (✉) · A. Liñán
E.T.S.I. Aeronáuticos, Universidad Politécnica de Madrid, Pl. Cardenal Cisneros 3, 28040 Madrid, Spain
E-mail: mario.sanchez@upm.es

A. Liñán
E-mail: amable.linan@upm.es

A. L. Sánchez
Dept. Ingeniería Térmica y de Fluidos, Universidad Carlos III de Madrid, 28911 Leganés, Spain
E-mail: asanchez@ing.uc3m.es

described in the boundary-layer approximation with small relative errors of order Re_j^{-2}, yielding a parameter-free description, to be computed numerically, that depends only on the shape of the velocity profile at the jet exit [1]. The jet is initially separated from the stagnant outer gas by a thin mixing layer whose thickness grows slowly with the downstream distance x', so that at distances of order $x' \sim Re_j a$ the effect of viscosity begins to modify significantly the value of the velocity at the jet axis. Downstream from this development region, i.e. at axial distances $x' \gg Re_j a$, the characteristic jet radius becomes much larger than a and the solution for the velocity approaches a self-similar constant-density description, due to Schlichting [2] for the round jet and to Bickley [3] for the planar jet, corresponding to the flow induced by a point source of momentum.

When the temperature of the gas at the jet exit T_j' differs from that of the ambient T_o' by a relative amount $(T_j' - T_o')/T_o'$ of order unity, density differences must be accounted for in the boundary-layer description of the jet development region, which, therefore, requires consideration of the energy conservation equation. These density differences become, however, small far from the jet development region, where the constant-density self-similar descriptions of the velocity field [2,3] remain valid. As shown by Yih [4], the small departures $(T' - T_o')$ of the temperature from the ambient value can also be described in the first approximation with the constant-density assumption, while effects of variable density in this region can be incorporated as small perturbations, a result due to Crane and Pack [5].

Of interest here are gaseous jets with extreme values of the initial jet-to-ambient temperature ratio, including hot jets with $T_j' \gg T_o'$ and cold jets with $T_o' \gg T_j'$. The associated density differences, which enter to modify the jet development region as described in [6] for hot jets, must also be taken into account for the description of the flow downstream, in a large region of axial and radial extents $x_c \gg Re_j a$ and $r_c \gg a$, where the relative density differences from the ambient value are of order of unity. Because of its relatively large size, in the description of this region the jet appears as a concentrated source of momentum and a source—for hot jets—or sink—for cold jets—of energy. We shall see that introduction of appropriate scales for the different variables, based on the jet fluxes of momentum and energy, yields a boundary-layer problem that depends on the Prandtl number Pr and on the temperature dependence of the transport properties, but it is otherwise free of parameters. Numerical integrations of the resulting problem provide a canonical solution that describes accurately the temperature and velocity in the far field of both planar and round hot jets and also of cold plane jets. The case of cold round jets will be found to be different, in that their far field solution in the region where the relative density changes are of order unity cannot be described as that induced by a point source of momentum.

The analysis presented here is restricted to steady laminar flows, which, therefore, limits the applicability of the results to configurations with moderately large values of the Reynolds number below the critical value at which the flow becomes unstable. Even though the theoretical stability studies [7,8] indicate that the onset of instability occurs at a critical Reynolds numbers given by $Re_j \simeq 30$ and $Re_j \simeq 40$ for planar and round jets, respectively, the experimental evidence seems to suggest that the critical values are considerably larger. For instance, in the early work of Andrade and Tsien [9] the laminar steady solution was found to exist for Reynolds numbers as large as $Re_j \sim 300$ and laminar jets have been obtained in more recent experiments for values of Re_j exceeding $Re_j = 600$ [10] and even $Re_j = 1000$ [11]. It is generally agreed that the development of the instability is slow, so that for values of the Reynolds number on the order of a few hundred unsteadiness is only noticeable far downstream, at very large distances on the order of a few hundred nozzle diameters [12,13], whereas the laminar steady solution remains valid at smaller distances from the jet exit. In the planar case, the resulting solution is more unstable than that of the round jet, as was experimentally confirmed in the early work of Andrade [14], who found the critical Reynolds number to be $Re_j \simeq 40$. Clearly, although the stability boundaries are expected to be modified in the presence of density differences, the laminar steady results presented below can be expected to be applicable for the description of configurations with moderately large values of Re_j, of interest in particular for small scale applications such as in micro and nano electromechanical systems. The ideas developed below could also find application in simplifying the description of cold and hot turbulent gas jets, an issue that should be investigated in the future.

2 Characteristic scales

Let us consider the large-Reynolds-number flow induced in a gas by a concentrated source of momentum of strength J that is also either a source or a sink of energy with strength Q. Of interest here is the region where the gas temperature and density differ from their ambient values T_o' and ρ_o' by relative amounts of order of unity. This region is slender for large values of the associated Reynolds number Re, to be defined precisely below

in (2), and can be, therefore, described in the boundary-layer approximation with small relative errors of order Re^{-2}. The corresponding conservation equations of momentum and energy provide the integral constraints

$$J = \int_0^\infty 2\pi^i \rho' u'^2 r'^i \, \mathrm{d}r' \quad \text{and} \quad Q = \pm \int_0^\infty 2\pi^i \rho' u' c_p (T' - T'_{\mathrm{o}}) r'^i \, \mathrm{d}r' \tag{1}$$

for the axial velocity u' and temperature T', with r' and x' denoting the radial and axial coordinates and $i = (0, 1)$ corresponding to the planar and axisymmetric configurations, respectively. In the formulation, ρ' represents the density and c_{p} is the specific heat at constant pressure, assumed to be constant. The positive and minus signs preceding the integral in the energy balance correspond, respectively, to the heat source and to the heat sink.

A straightforward order-of-magnitude analysis of (1) determines the characteristic value of the velocity $u_{\mathrm{c}} = j/m$ and of the radius $r_{\mathrm{c}} = [m^2/(\rho'_{\mathrm{o}} j)]^{1/(i+1)}$ in the region where the temperature differences $T' - T'_{\mathrm{o}}$ are of order T'_{o}. In order to simplify the writing, we have introduced the normalised quantities $j = J/(2\pi^i)$ and $m = Q/(2\pi^i c_{\mathrm{p}} T'_{\mathrm{o}})$, the latter having dimensions of a mass flux. The associated Reynolds number $Re = \rho'_{\mathrm{o}} u_{\mathrm{c}} r_{\mathrm{c}}/\mu'_{\mathrm{o}}$, a large quantity in the present development, is given by

$$Re = m/\mu'_{\mathrm{o}} \ \ (i = 0) \quad \text{and} \quad Re = (\rho'_{\mathrm{o}} j)^{1/2}/\mu'_{\mathrm{o}} \ \ (i = 1), \tag{2}$$

where μ'_{o} represents the ambient value of the viscosity. In order to complete the set of characteristic scales in this region, the balance between convection and diffusion can be employed to give $x_{\mathrm{c}} = Re\, r_{\mathrm{c}}$ for the axial extent of this region, where the characteristic radial velocity is $v_{\mathrm{c}} = \mu'_{\mathrm{o}}/(\rho'_{\mathrm{o}} r_{\mathrm{c}})$, as follows from the continuity balance.

Before proceeding with the analysis, it is of interest to compare the different scales of this region with those found in the development region of hot and cold jets of initial radius a, based on the characteristic values u'_{j}, T'_{j}, ρ'_{j} and μ'_{j} of the velocity, temperature, density and viscosity at the jet exit. In relating these scales with those found downstream, the power law $\mu'_{\mathrm{j}}/\mu'_{\mathrm{o}} = (T'_{\mathrm{j}}/T'_{\mathrm{o}})^\sigma$ is assumed for the temperature dependence of the transport properties, where the exponent σ takes for nonionised gases a value between $\sigma = 0.5$ and $\sigma = 0.7$, and the estimates $J \sim \rho'_{\mathrm{j}} u'^2_{\mathrm{j}} a^2$ and $Q \sim \pm \rho'_{\mathrm{j}} u'_{\mathrm{j}} c_{\mathrm{p}} (T'_{\mathrm{j}} - T'_{\mathrm{o}}) a^2$ are used for the jet fluxes of momentum and energy.

For a hot jet $T'_{\mathrm{j}} \gg T'_{\mathrm{o}}$, so that the expression for the heat flux simplifies to $Q \sim \rho'_{\mathrm{j}} u'_{\mathrm{j}} c_{\mathrm{p}} T'_{\mathrm{j}} a^2$, where $\rho'_{\mathrm{j}} T'_{\mathrm{j}} = \rho'_{\mathrm{o}} T'_{\mathrm{o}}$ as dictated by the equation of state, thereby yielding

$$\frac{u_{\mathrm{c}}}{u'_{\mathrm{j}}} \sim \left(\frac{T'_{\mathrm{j}}}{T'_{\mathrm{o}}} \right)^{-1}, \quad \frac{r_{\mathrm{c}}}{a} \sim \left(\frac{T'_{\mathrm{j}}}{T'_{\mathrm{o}}} \right)^{1/(1+i)} \quad \text{and} \quad \frac{x_{\mathrm{c}}}{Re_{\mathrm{j}} a} \sim \left(\frac{T'_{\mathrm{j}}}{T'_{\mathrm{o}}} \right)^{\sigma+2/(1+i)}. \tag{3}$$

Clearly, the size of the far field region of hot jets is much larger than that of the jet development region and its characteristic velocity is much smaller. Note that, because of the downstream temperature increase, the Reynolds number increases with distance to give $Re \sim (T'_{\mathrm{j}}/T'_{\mathrm{o}})^{\sigma+1/(1+i)} Re_{\mathrm{j}}$ in the far field region.

For a cold jet, $T'_{\mathrm{j}} \ll T'_{\mathrm{o}}$ and the simplified estimate $Q \sim \rho'_{\mathrm{j}} u'_{\mathrm{j}} c_{\mathrm{p}} T'_{\mathrm{o}} a^2$ applies. When this is used in the expressions for the scales of the far field region one obtains

$$\frac{u_{\mathrm{c}}}{u'_{\mathrm{j}}} \sim O(1), \quad \frac{r_{\mathrm{c}}}{a} \sim \left(\frac{T'_{\mathrm{o}}}{T'_{\mathrm{j}}} \right)^{1/(1+i)} \quad \text{and} \quad \frac{x_{\mathrm{c}}}{Re_{\mathrm{j}} a} \sim \left(\frac{T'_{\mathrm{o}}}{T'_{\mathrm{j}}} \right)^{(1-i)/(1+i)-\sigma}, \tag{4}$$

whereas the characteristic Reynolds number is given by $Re \sim (T'_{\mathrm{o}}/T'_{\mathrm{j}})^{-\sigma-i/(1+i)} Re_{\mathrm{j}} \ll Re_{\mathrm{j}}$. The last expression in (4) indicates that, for the values $\sigma < 1$ that characterise the temperature dependence of the viscosity of nonionised gases, $x_{\mathrm{c}} \gg Re_{\mathrm{j}} a$ for plane cold jets ($i = 0$), so that the jet can be considered as a concentrated source of momentum and a sink of energy when describing the far field region. For $i = 1$, however, one finds $x_{\mathrm{c}} \ll Re_{\mathrm{j}} a$ regardless of the value of $\sigma > 0$, thereby precluding the applicability of the point-source analysis, which relies on the assumption that the far field is much larger than the jet development region. The description given below, therefore, does not apply to cold round jets, whose far field analysis can be anticipated to necessitate specific consideration of the solution in the jet development region, as discussed below.

3 Formulation

Using the above scales to define dimensionless velocity components $u = u'/u_c$ and $v = v'/v_c$ and dimensionless coordinates $r = r'/r_c$ and $x = x'/x_c$ reduces the boundary layer equations to

$$\frac{\partial}{\partial x}(\rho u) + \frac{1}{r^i}\frac{\partial}{\partial r}(\rho r^i v) = 0, \tag{5}$$

$$\rho u \frac{\partial u}{\partial x} + \rho v \frac{\partial u}{\partial r} = \frac{1}{r^i}\frac{\partial}{\partial r}\left(r^i \mu \frac{\partial u}{\partial r}\right), \tag{6}$$

$$\rho u \frac{\partial T}{\partial x} + \rho v \frac{\partial T}{\partial r} = \frac{1}{Pr}\frac{1}{r^i}\frac{\partial}{\partial r}\left(r^i \mu \frac{\partial T}{\partial r}\right), \tag{7}$$

where $T = T'/T_o'$, $\rho = \rho'/\rho_o'$ and $\mu = \mu'/\mu_o'$, and Pr represents the Prandtl number, assumed to be constant in the analysis. Viscous dissipation has been neglected in the energy equation, an appropriate simplification for low-Mach-number jets. The above equations need to be supplemented with the quasi-isobaric form of the equation of state

$$\rho T = 1, \tag{8}$$

and with the presumed power law

$$\mu = T^\sigma, \tag{9}$$

for the temperature dependence of the transport properties. Appropriate boundary conditions for $x > 0$ are given by

$$r = 0 : \frac{\partial u}{\partial r} = v = \frac{\partial T}{\partial r} = 0,$$

$$r \to \infty : u = T - 1 = 0. \tag{10}$$

Note that these boundary conditions can be used in radial integrations of the conservative form of (6) and (7) to give the integral conservation laws

$$\int_0^\infty \rho u^2 r^i \, dr = 1 \text{ and } \int_0^\infty \rho u(T - 1)r^i \, dr = \pm 1, \tag{11}$$

previously anticipated in (1). The boundary conditions at the jet exit for (5–7) are derived below by investigating the flow field at $x \ll 1$, where self-similar solutions exist for the source of heat and for the planar sink of heat, and no solution is found for the axisymmetric sink of heat.

3.1 The near-field solution for the point source of heat

For a point source of heat, both the temperature and the velocity near the source diverge according to $u \sim T \sim x^{-(i+1)/[2+\sigma(i+1)]}$ in a relatively thin jet region of characteristic radius $r \sim x^{1/[2+\sigma(i+1)]}$, as can be seen by using (11) along with the convection–diffusion balance $\rho u^2/x \sim \mu u/r^2$. Since the resulting temperature becomes asymptotically large, the solution corresponds in the first approximation to the self-similar boundary-layer flow induced by a point source of momentum and heat in a gas of vanishing temperature [15–17], which arises in the description of high-temperature gas jets downstream from their jet-development region [6]. Because of the temperature dependence of the transport properties, in this limit of zero outer temperature heat conduction and shear stresses vanish at a finite radial distance r_f, and a front solution emerges.

The above scalings suggest the rescaled coordinate $\xi = r/x^{1/[2+\sigma(1+i)]}$, along with the temperature $\theta = x^{(1+i)/[2+\sigma(1+i)]}T$ and the stream function $\psi = x^{(1+i)/[2+\sigma(1+i)]}f(\xi)$, defined such that $\rho u = f_\xi/\xi^i$ and
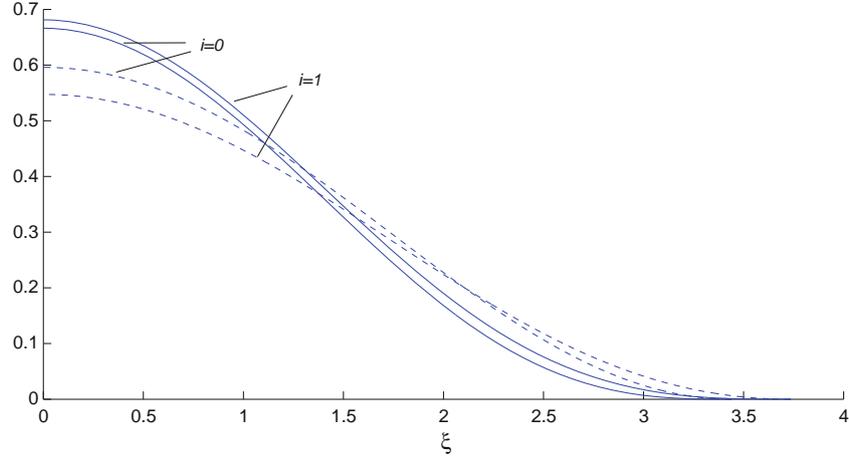
Fig. 1 Profiles of temperature θ (*dashed curves*) and velocity U (*solid curves*) obtained from integrations of 12 for $Pr = 0.7$ and $\sigma = 0.5$

$\rho r^i v = -x^{[i-1-\sigma(1+i)]/[2+\sigma(1+i)]}[(1+i)f - \xi f_\xi]/[2+\sigma(1+i)]$, where the subscript ξ indicates differentiation with respect to this variable. As shown in [6], the resulting momentum and energy equations

$$\xi^i \theta^\sigma \left(\frac{\theta f_\xi}{\xi^i}\right)_\xi + \frac{(1+i)f}{2+\sigma(1+i)}\left(\frac{\theta f_\xi}{\xi^i}\right) = 0 \quad \text{and} \quad \xi^i \theta^\sigma \theta_\xi + \frac{(1+i)Prf}{2+\sigma(1+i)}\theta = 0. \tag{12}$$

can be integrated with boundary conditions $\theta = \theta f_\xi = 0$ at $\xi = \xi_f$ and $\theta_\xi = (\theta f_\xi/\xi^i)_\xi = 0$ at $\xi = 0$ and with the integral constraints $\int_0^{\xi_f} f_\xi^2 \theta/\xi^i \mathrm{d}\xi = \int_0^{\xi_f} f_\xi \theta \mathrm{d}\xi = 1$ to determine the selfsimilar temperature $\theta(\xi)$ and velocity $U(\xi) = x^{(1+i)/[2+\sigma(1+i)]}u = \theta f_\xi/\xi^i$ profiles, along with the front location $\xi_f = r_f/x^{1/[2+\sigma(1+i)]}$, beyond which $\theta = U = 0$. These selfsimilar profiles, given in Fig. 1 for $Pr = 0.7$ and $\sigma = 0.5$, can be used in constructing the initial profiles

$$T = 1 + x^{-(1+i)/[2+\sigma(1+i)]}\theta\left\{r/x^{1/[2+\sigma(1+i)]}\right\} \quad \text{and} \quad u = x^{-(1+i)/[2+\sigma(1+i)]}U\left\{r/x^{1/[2+\sigma(1+i)]}\right\} \tag{13}$$

for the integration of (5–7).

3.2 The near-field solution for the point sink of heat

For a point sink of heat, the negative sign must be selected in the second equation of (11). The solution near the singularity will be described below for $i = 0$, while no solution can be obtained for the case $i = 1$, a finding that is consistent with the scaling arguments given below (4), which indicate that the point-source analysis is not applicable to the far-field description of cold round jets.

For the plane jet, the solution for $x \ll 1$ shows a two-layer structure with the momentum and energy fluxes concentrated in a narrow cold core that is surrounded by thicker layers of warm gas. In the cold core ($T \ll 1$), the integral conservation equations of momentum and energy given in (11) reduce to $\int_0^\infty (u^2/T)\mathrm{d}r = \int_0^\infty (u/T)\mathrm{d}r = 1$. Both the conditions can be simultaneously fulfilled only if the velocity satisfies $u - 1 \ll 1$. Therefore, across the layers of warm gas that surround the cold jet the velocity evolves from an ambient zero value to reach $u = 1$ as $r \to 0$. The solution is determined by a balance between convection and molecular transport to be described in terms of the selfsimilar variable $\eta = r/\sqrt{x}$ and the stream function $\psi = \sqrt{x}F(\eta)$. The problem reduces to that of integrating the momentum and energy equations

$$\begin{cases} [T^\sigma(TF_\eta)_\eta]_\eta + F(TF_\eta)_\eta/2 = 0 \\ (T^\sigma T_\eta)_\eta + PrFT_\eta/2 = 0 \end{cases} \tag{14}$$

with boundary conditions $T = 1$ and $TF_\eta = 0$ as $\eta \to \infty$ and $T = 0$ and $TF_\eta = 1$ as $\eta \to 0$, with the subscript η representing differentiation with respect to this variable. The solution close to the axis

$$T = \left(\frac{Pr(1+\sigma)\eta^2}{2(1-\sigma)}\right)^{1/(1+\sigma)} \left(1 + C_1 \eta^{(-\sigma+\sqrt{2-\sigma^2})/(1+\sigma)}\right) \tag{15}$$

$$TF_\eta = 1 - C_2 \eta^{2/(1+\sigma)+(1-Pr)/Pr} \tag{16}$$

is taken into account in the numerical integration, where the constants C_1 and C_2 are selected in the shooting procedure to satisfy the boundary conditions at $\eta \to \infty$, giving for instance $C_1 = -6.972$ and $C_2 = -1.850$ for $\sigma = 0.5$ and $Pr = 0.7$.

The integration determines the profiles of temperature T and velocity $\bar{U} = TF'$ shown in Fig. 2, to be used below in constructing the initial velocity and temperature profiles for the integration of (5–7). This outer solution fails as the temperature vanishes at the axis. In the resulting cold jet $u - 1 \ll 1$, so that both the equations in (11) reduce to the mass conservation equation

$$\int_0^\infty T^{-1} dr = 1, \tag{17}$$

which provides the scales $r \sim T \sim 1 - u \sim x^{1/(1-\sigma)}$ when combined with the proviso that convective and diffusive terms be also balanced in this region. Introducing the selfsimilar variable $\zeta = r/x^{1/(1-\sigma)}$ and the rescaled temperature $\Theta = x^{-1/(1-\sigma)}T$ into (7) yields

$$\left(\frac{\zeta}{\Theta}\right)_\zeta = \frac{1-\sigma}{Pr}\left(\Theta^{\sigma-1}\Theta_\zeta\right)_\zeta \tag{18}$$

to be integrated with the symmetry condition $\Theta_\zeta = 0$ at $\zeta = 0$ and the matching condition with the outer solution $\Theta = \left(\frac{Pr(1+\sigma)}{2(1-\sigma)}\right)^{1/(1+\sigma)} \zeta^{2/(1+\sigma)}$ as $\zeta \to \infty$ determined with use made of (15). Eq. (18) can be readily integrated to give

$$\Theta = \left(A + \frac{Pr(1+\sigma)}{2(1-\sigma)}\zeta^2\right)^{1/(1+\sigma)}, \tag{19}$$

where the constant

$$A = \left[\frac{\Gamma\left(\frac{3}{2}\right)\Gamma\left(\frac{1-\sigma}{2(1+\sigma)}\right)}{\Gamma\left(\frac{1}{1+\sigma}\right)}\left(\frac{2(1-\sigma)}{Pr(1+\sigma)}\right)^{1/2}\right]^{2(1+\sigma)/(1-\sigma)} \tag{20}$$

is selected to satisfy the integral condition $\int_0^\infty \Theta^{-1}d\zeta = 1$ derived from (17), with $\Gamma()$ representing the Gamma function [18].

The above asymptotic expansions in the cold core and in the surrounding warm layers can be combined to give

$$T = T\left(\frac{r}{x^{1/2}}\right) + x^{1/(1-\sigma)}\Theta\left(\frac{r}{x^{1/(1-\sigma)}}\right) - \left(\frac{Pr}{2}\frac{1+\sigma}{1-\sigma}\right)^{1/(1+\sigma)}\left(\frac{r}{x^{1/2}}\right)^{2/(1+\sigma)} \tag{21}$$

$$u = \bar{U}\left(\frac{r}{x^{1/2}}\right),$$

as boundary conditions at $x \ll 1$ for the integration of (5–7). Note that the velocity profile could be in principle corrected near the axis by accounting for the small velocity changes $1 - u \sim x^{1/(1-\sigma)}$ that occur across the cold jet, but this higher-order correction in the boundary condition $x = 0$ is unnecessary, in that it does not lead to appreciable improvements in the solution.

As previously mentioned, no near-field solution can be found in the axisymmetric case. To see this, note that consideration of the integral conditions (11) together with the balance between convection and conduction
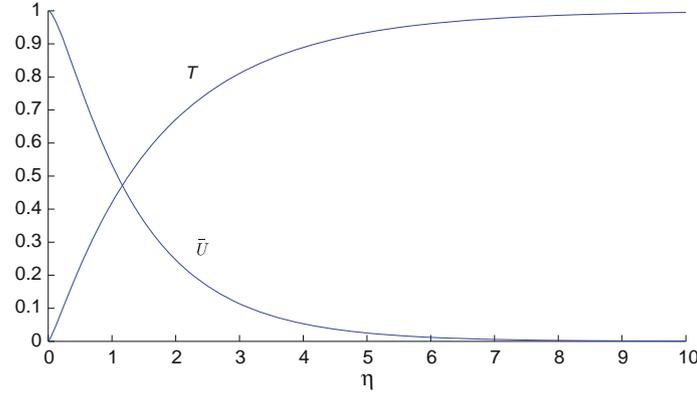
Fig. 2 Profiles of temperature T and velocity $\bar{U}$ obtained from the integration of 14 for $Pr = 0.7$ and $\sigma = 0.5$

leads in this case to the diverging values $r^2 \sim T \sim x^{-1/\sigma}$, which are not consistent with the existence of a concentrated sink of energy at the origin. Since no solution can be found for the near field, the boundary-layer formulation for the axisymmetric flow induced by a point source of momentum that is simultaneously a sink of energy remains incomplete. This finding further supports the idea that a solution based on point singularities does not apply to the description of the far field of cold round jets, in agreement with the previous scaling arguments given below (4).

4 Gaseous jets with extreme values of the initial temperature

The variable-density flow induced by a concentrated source of momentum is determined by integration of (5–7) supplemented with (8) and (9) and subject to the boundary conditions given in (10) and at $x \ll 1$ given in (13) for the heat source and in (21) for the planar heat sink. The solution is free of parameters, except for the gas transport properties, defined by the Prandtl number Pr and the exponent σ of the presumed temperature dependence of the viscosity, given in (9). In particular, the values $Pr = 0.7$ and $\sigma = 0.5$ were selected in the integrations, giving the results shown as solid lines in Figs. 3–8. The results were tested to be independent of the location $x \ll 1$ used in evaluating the initial profiles (13) and (21), with the value $x = 0.001$ selected for the computations in the figures. The plots include the downstream evolution of the temperature and velocity along the axis as well as characteristic radial profiles at different axial locations. The solution evolves from the near-source self-similar solutions at $x \ll 1$ to the far-field constant-density solutions for $x \gg 1$

$$u = \frac{8}{x} \frac{64/6}{\left[64/6 + (r/x)^2\right]^2} \quad \text{and} \quad T - 1 = \pm \frac{1}{x} \frac{(1 + 2Pr)/4}{\left[1 + 6(r/x)^2/64\right]^{2Pr}} \tag{22}$$

for the round jet [2,4] and

$$u = \frac{3}{2(9x)^{1/3}} \left[1 - \tanh^2\left(\frac{3}{2}\frac{r}{(9x)^{2/3}}\right)\right] \quad \text{and} \quad T - 1 = \pm \frac{2}{(9x)^{1/3}} \frac{\left[\cosh\left(\frac{3}{2}\frac{r}{(9x)^{2/3}}\right)\right]^{-2Pr}}{B(1 + 2Pr, 1/2)} \tag{23}$$

for the plane jet [3,4], where $B()$ represents the Beta function [18].

As mentioned above, these variable-density flows induced by concentrated sources find application for the description of gaseous jets with either very small or very large values of the jet-to-ambient temperature ratios in the relatively large far-field region where nonnegligible density differences are found, located upstream from the region of applicability of the constant-density descriptions (22) and (23). The numerical solution for these very cold or very hot jets can be obtained by integrating the jet boundary-layer Eqs. (5–7) with the boundary conditions given in (10). The boundary conditions at $x = 0$ are those found at the jet exit, given in dimensional form by $u' = u'_j(r')$ and $T' = T'_j(r')$ for $r' < a$ and $u' = 0$ and $T' = T'_o$ for $r' > a$, with u'_j and T'_j representing the profiles of temperature and velocity at the jet exit. If these are assumed to be uniform, then the dimensionless form of the boundary conditions at $x = 0$ for integration of (5–7) reduces to
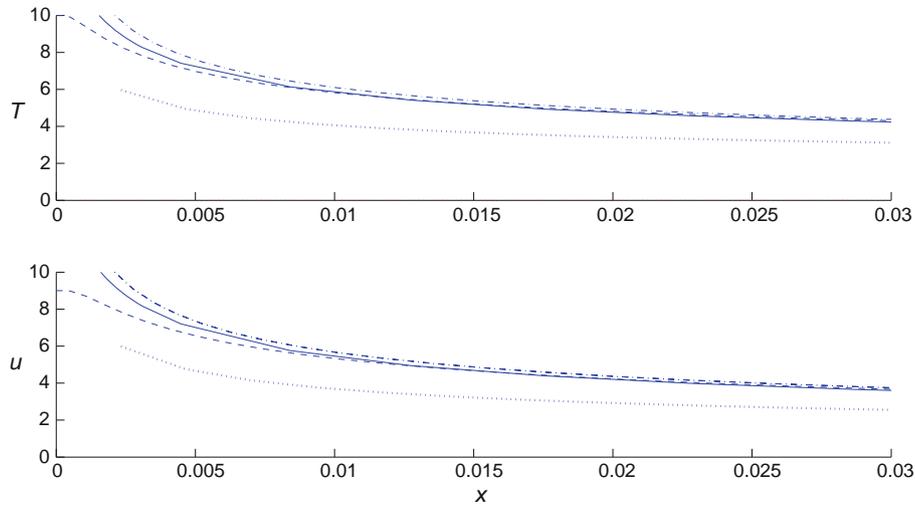
Fig. 3 The evolution of the temperature T (*upper plot*) and velocity u (*lower plot*) along the axis as obtained for $Pr = 0.7$, $\sigma = 0.5$ and $i = 0$ from integrations of (5–7) with the point-source boundary conditions at $x \ll 1$ (13) (*solid curves*) and with the hot-jet boundary conditions at $x = 0$ (24) for $T_j = 10$ (*dashed curves*) and $T_j = 20$ (*dot-dashed curves*). The dotted lines represent the constant-density solution $u = [3/(8x)]^{1/3}$ and $T = 1 + 2/[(9x)^{1/3} B(1 + 2Pr, 1/2)]$
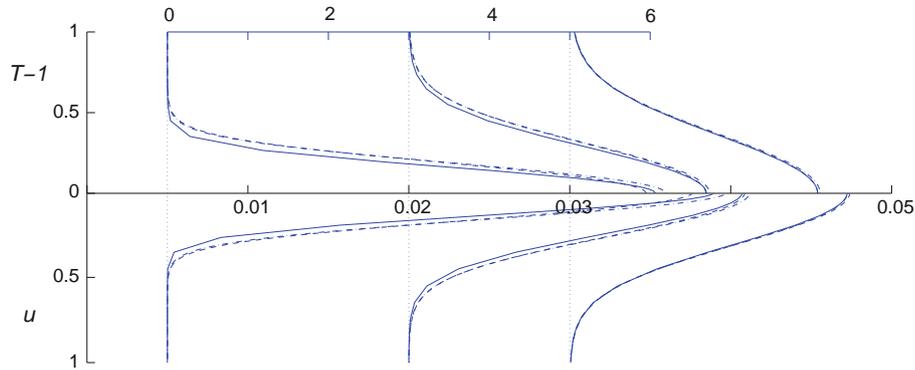

Fig. 4 The profiles of temperature $T - 1$ (*upper half of the plot*) and velocity u (*lower half of the plot*) for $Pr = 0.7$, $\sigma = 0.5$ and $i = 0$ obtained from integrations of (5–7) with the point-source boundary conditions at $x \ll 1$ (13) (*solid curves*) and with the hot-jet boundary conditions at $x = 0$ (24) for $T_j = 10$ (*dashed curves*) and $T_j = 20$ (*dot-dashed curves*); the scale for the velocity and temperature is indicated for the profiles at $x = 0.05$
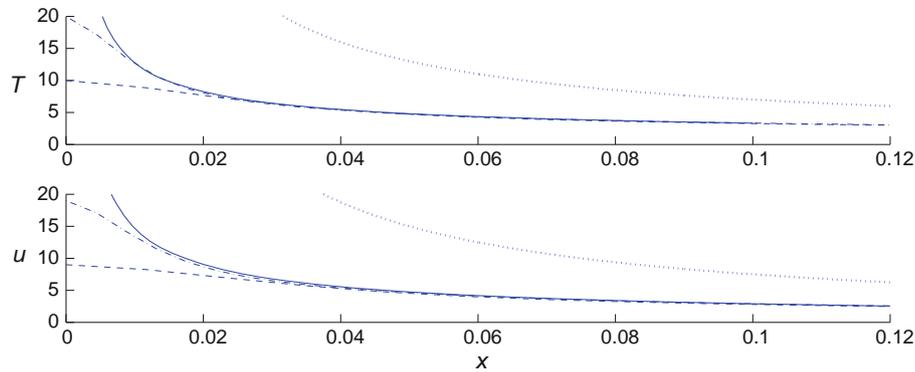

Fig. 5 The evolution of the temperature T (*upper plot*) and velocity u (*lower plot*) along the axis as obtained for $Pr = 0.7$, $\sigma = 0.5$ and $i = 1$ from integrations of (5–7) with the point-source boundary conditions at $x \ll 1$ (13) (*solid curves*) and with the hot-jet boundary conditions at $x = 0$ (24) for $T_j = 10$ (*dashed curves*) and $T_j = 20$ (*dot-dashed curves*). The dotted curves represent the constant-density predictions $u = 3/(4x)$ and $T - 1 = (1 + 2Pr)/(4x)$
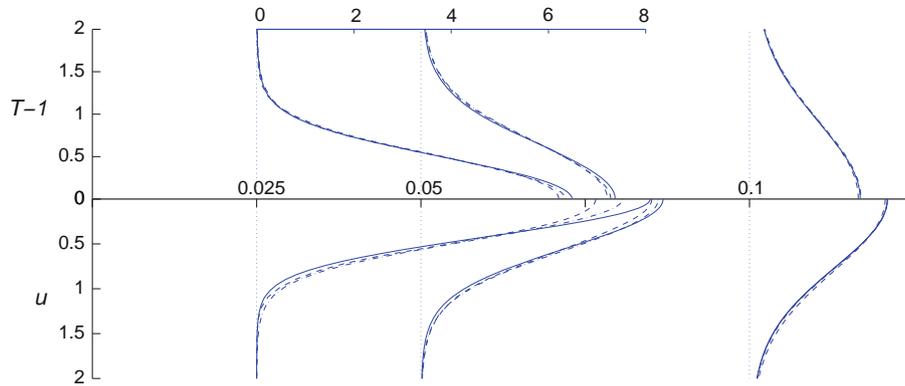
Fig. 6 The profiles of temperature $T - 1$ (*upper half of the plot*) and velocity u (*lower half of the plot*) for $Pr = 0.7$, $\sigma = 0.5$ and $i = 1$ obtained from integrations of (5–7) with point-source boundary conditions at $x \ll 1$ (13) (*solid curves*) and with the hot-jet boundary conditions at $x = 0$ (24) for $T_j = 10$ (*dashed curves*) and $T_j = 20$ (*dot-dashed curves*); the scales for the velocity and temperature are indicated for the profiles at $x = 0.05$ on each plot
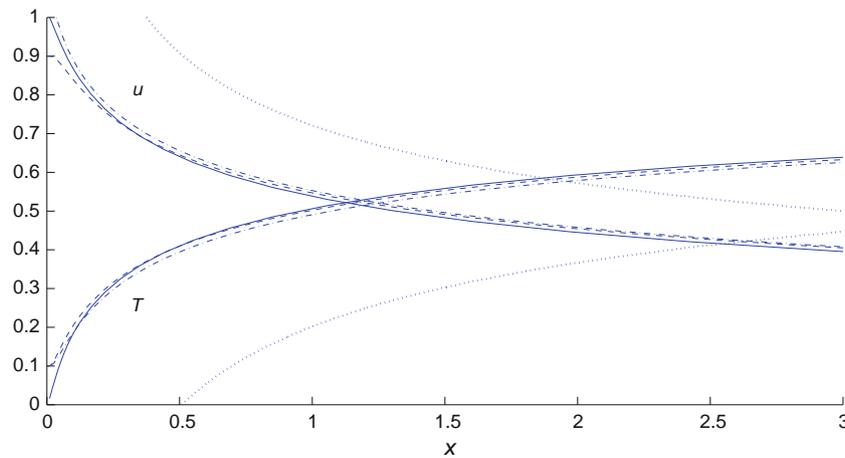

Fig. 7 The evolution of the temperature T and velocity u along the axis as obtained for $Pr = 0.7$, $\sigma = 0.5$ and $i = 0$ from integrations of (5–7) with the point-source boundary conditions at $x \ll 1$ (21) (*solid curves*) and with the cold-jet boundary conditions at $x = 0$ (24) (*dashed curves*) and (25) (*dot-dashed curves*) with $T_j = 0.1$. The dotted lines represent the constant-density solution $u = [3/(8x)]^{1/3}$ and $T = 1 - 2/[(9x)^{1/3}B(1 + 2Pr, 1/2)]$
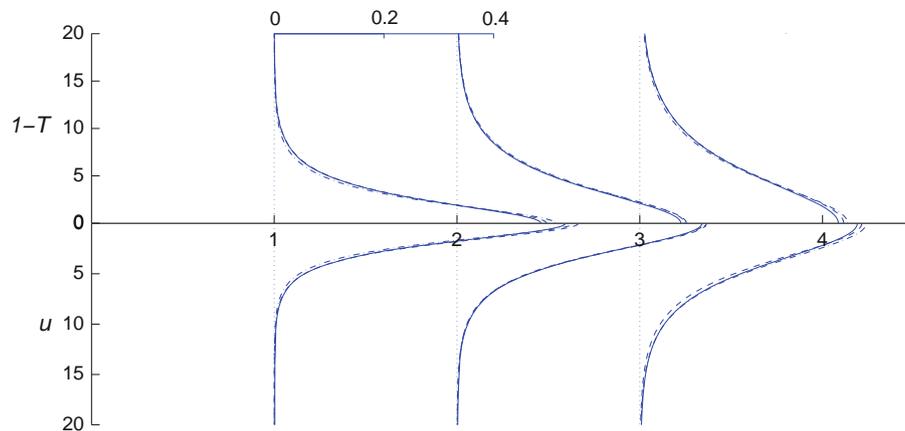

Fig. 8 The profiles of temperature $1 - T$ (*upper half of the plot*) and velocity u (*lower half of the plot*) for $Pr = 0.7$, $\sigma = 0.5$ and $i = 0$ obtained from integrations of (5–7) with the point-source boundary conditions at $x \ll 1$ (21) (*solid curves*) and with the cold-jet boundary conditions at $x = 0$ (24) (*dashed curves*) and (25) (*dot-dashed curves*) with $T_j = 0.1$. The scale for the velocity and temperature is indicated for the profiles at $x = 1$

$$\begin{cases} r < r_{\mathrm{j}} : u = \pm(T_{\mathrm{j}} - 1), \quad T = T_{\mathrm{j}} \\ r > r_{\mathrm{j}} : u = 0, \quad T = 1 \end{cases} \tag{24}$$

where $T_{\mathrm{j}} = T_{\mathrm{j}}'/T_{\mathrm{o}}'$ is the dimensionless jet temperature and $r_{\mathrm{j}} = a/r_{\mathrm{c}} = [T_{\mathrm{j}}/(T_{\mathrm{j}} - 1)^2]^{1/(1+i)}$ is the initial jet radius, which becomes small for extreme values of T_{j} corresponding to very cold and very hot jets.

The governing Eqs. (5–7) were integrated with an implicit marching procedure, second-order accurate in x and r. A non-uniform grid with minimum spacing $\delta x = 3 \times 10^{-3}$ near the entrance and $\delta r = 3.5 \times 10^{-4}$ near the axis was used, and the results were checked to be grid-independent by comparison with results obtained with finer grids in sample computations. The accuracy of the final numerical solution was tested by evaluating the integral constraints given in (11). The errors in the momentum and energy fluxes were checked to be below 1% at all x stations.

Results corresponding to hot jets with initial temperatures $T_{\mathrm{j}} = 10$ and $T_{\mathrm{j}} = 20$ are shown in Figs. 3 and 4 for the planar configuration and in Figs. 5 and 6 for the axisymmetric configuration. As can be seen, the point-source solution describes accurately the hot jet in the region where the temperature variations with respect to the ambient value $T - 1$ are of the order of unity, except in a fairly small initial region of jet development. This region is noticeably smaller for the plane jet, as could have been anticipated by noting that the initial value of the jet radius expressed in dimensionless form, given approximately $r_{\mathrm{j}} = a/r_{\mathrm{c}} \simeq T_{\mathrm{j}}^{-1/(1+i)}$ for $T_{\mathrm{j}} \gg 1$, is much smaller for $i = 0$. As expected, the agreement with the point-source results is better for the larger value $T_{\mathrm{j}} = 20$ considered, although satisfactory results are also obtained for $T_{\mathrm{j}} = 10$.

Figures 3 and 5 include the constant-density predictions $u = [3/(8x)]^{1/3}$ and $T - 1 = 2/[(9x)^{1/3}B(1 + 2Pr, 1/2)]$ $(i = 0)$ and $u = 3/(4x)$ and $T - 1 = (1 + 2Pr)/(4x)$ $(i = 1)$ for the variation of u and T along the axis obtained by evaluating (22) and (23) at $r = 0$. As can be seen, in the range of streamwise distances considered, the density variations are too large for the constant-density approximation to be accurate. The applicability of (22) and (23) is, therefore, postponed to the region $x \gg 1$ where $T - 1 \ll 1$. These leading-order far-field descriptions could be improved by introduction of a virtual origin, with a value that would be different from that encountered in constant-density jets [1].

The case of a planar cold jet is considered in Figs. 7 and 8, where the flow induced by a point sink of heat is compared with the boundary-layer solution for a moderately cold jet with $T_{\mathrm{j}} = 0.1$. Besides a uniform velocity profile at the jet exit $u = 1 - T_{\mathrm{j}}$, numerical integrations were also performed for the case of a Poiseuille velocity distribution, for which the boundary conditions at $x = 0$ become

$$\begin{cases} r < r_{\mathrm{j}} : u = \frac{5}{4}(1 - T_{\mathrm{j}})[1 - (r/r_{\mathrm{j}})^2], \quad T = T_{\mathrm{j}} \\ r > r_{\mathrm{j}} : u = 0, \quad T = 1 \end{cases} \tag{25}$$

with the initial jet radius given by $r_{\mathrm{j}} = a/r_{\mathrm{c}} = (6/5)T_{\mathrm{j}}/(1 - T_{\mathrm{j}})^2$. In view of the figure, it is clear that the flow induced by a point source of momentum that is simultaneously a sink of heat is an excellent approximation for a cold jet with a moderately small value of $T_{\mathrm{j}} = 0.1$, with errors remaining below 5% for $x \gtrsim 0.1$. As occurs with the case of hot jets, the self-similar solutions of Bickley and Yih [3,4], indicated by the dotted lines in Fig. 7, are not acceptable approximations in this region of significant density variations.

5 Conclusions

We have seen that gaseous jets with extreme initial temperatures present significant density variations far downstream from the region of jet development. This region is sufficiently large that the effect of the jet appears as that of a concentrated source of momentum that is simultaneously either a source of energy (for the hot jet) or a sink of energy (for the cold jet). The problem was formulated by nondimensionalising the boundary-layer equations with the scales determined from the source fluxes of momentum and energy. In order to complete the formulation, the near-source field was investigated, providing appropriate self-similar descriptions that were used as boundary conditions at $x \ll 1$ for the integration of the boundary-layer equations. As seen in Figs. 3–8, the resulting canonical solutions, which depend on the gas transport properties through the values of Pr and σ but are otherwise free of parameters, constitute a very accurate description for cold and hot jets downstream from the region of jet development.

The scalings presented in (4) indicate that for cold round jets the axial extent of the region of jet development is not small compared with that of the far field region where density differences are comparable to the ambient value. This is further investigated in Fig. 9, which shows results of numerical integrations for $i = 1$
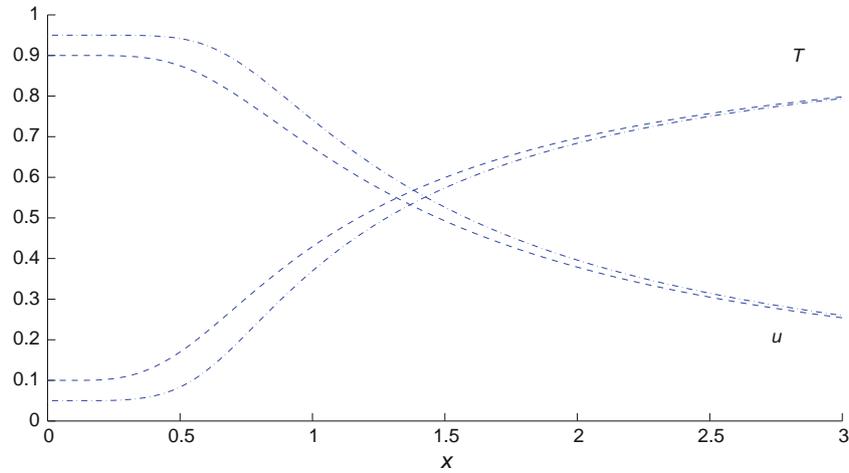
Fig. 9 The evolution of the temperature T and velocity u along the axis as obtained for $Pr = 0.7$, $\sigma = 0.5$ and $i = 1$ from integrations of (5–7) with the cold-jet boundary conditions at $x = 0$ (24) for $T_j = 0.1$ (*dashed curves*) and for $T_j = 0.05$ (*dot-dashed curves*)

and two different initial temperatures $T_j = (0.05, 0.1)$. As can be seen, the jet structure in this case is different from that seen in Fig. 7 for the plane jet, in that the cold round jet shows a relatively long region of initial jet development where the temperature and velocity at the axis remain unperturbed. The length of this region is clearly not negligible compared with the length of the downstream region where the temperature increases to reach values of the order of unity. Correspondingly, the integrations indicate that the characteristic value of the jet radius at the end of the development region, i.e. at $x \simeq 0.5$ for the jets considered in Fig. 9, is comparable to that found in the far field region, so that when describing this latter region the jet cannot be viewed as a point singularity placed at the origin.

Future work should, therefore, investigate the region of jet development to determine the boundary conditions that apply upstream from the far field region in terms of the small value of T_j'/T_o'. Front solutions similar to those found in hot jets [6] are likely to emerge in the limit $T_j'/T_o' \ll 1$ of very cold jets, thereby complicating the description. Previous analyses of boundary-layer development over cylinders [19,20] may be relevant in obtaining asymptotic descriptions for the flow downstream from the development region, which can be anticipated to involve slowly converging expansions in terms of logarithms of the rescaled downstream distance.

References

1. Revuelta, A., Sánchez, A.L., Liñán, A.: The virtual origin as a first-order correction for the far-field description of laminar jets. Phys. Fluids **14**, 1821–1824 (2002)
2. Schlichting, H.: Laminare strahlausbreitung. Z. Angew. Math. Mech. **13**, 260–263 (1933)
3. Bickley, W.: The plane jet. Phil. Mag. **23**, 727–731 (1937)
4. Yih, C.S.: Temperature distribution in a steady laminar preheated air jet. J. Appl. Mech. **18**, 381–382 (1950)
5. Crane, L.J., Pack, D.C.: The laminar and turbulent mixing of jets of compressible fluid. Part I flow far from the orifice. J. Fluid Mech. **2**, 449–455 (1957)
6. Sánchez-Sanz, M., Sánchez, A.L., Liñán, A.: Fronts in high-temperature laminar gas jets. J. Fluid Mech. **547**, 257–266 (2006)
7. Garg, V.K.: Spatial stability of the non-parallel Bickley jet. J. Fluid Mech. **102**, 127–140 (1981)
8. Morris, P.J.: The spatial viscous instability of axisymmetric jets. J. Fluid Mech. **77**, 511–529 (1976)
9. Andrade, E.N., Tsien, L.C.: The velocity distribution in a liquid into liquid jet. Proc. Phil. Soc. London **49**, 381–391 (1937)
10. O'Neill, P., Soria, J., Honnery, D.: The stability of low Reynolds number round jets. Exp. Fluids **36**, 473–483 (2004)
11. Rankin, G.W., Sridhar, K., Arulraja, M., Kumar, K.R.: An experimental investigation of laminar axisymmetric submerged jets. J. Fluid Mech. **133**, 217–231 (1983)
12. Reynolds, A.J.: Observations of a liquid-into-liquid jet. J. Fluid Mech. **14**, 552–556 (1962)
13. Koller-Milojevic, D., Schneider, W.: Free and confined jets at low Reynolds numbers. Fluid Dyn. Res. **12**, 307–322 (1993)
14. Andrade, E.N.: The velocity distribution in a liquid into liquid jet. The plane jet. Proc. Phil. Soc. London **51**, 784–793 (1939)

15. Bobnev, A.A.: Exact solution for a high-temperature jet. J. Appl. Mech. Tech. Phys. (Historical Archive) **23**, 647–651 (1982)
16. Bobnev, A.A.: Class of self-similar solutions for a high-temperature axisymmetric jet. J. Appl. Mech. Tech. Phys. (Historical Archive) **26**, 490–496 (1985)
17. Bobnev, A.A.: Class of self-similar solutions for high-temperature plane and fan jets. High Temp. **24**, 212–219 (1986)
18. Abramowitz, M., Stegun, A.: Handbook of Mathematical Functions. Dover, New York (1965)
19. Stewartson, K.: The asymptotic boundary layer on a circular cylinder in axial incompressible flow. Quart. J. Appl. Math **13**, 113–122 (1955)
20. Glauert, M.B., Lighthill, M.J.: The axisymmetric boundary layer on a long thin cylinder. Proc. R. Soc. London A **230**, 188–203 (1955)